Time-Resolved Photodissociation of Singly Protonated Peptides with an Arginine at the N-Terminus: A Statistical Interpretation

So Hee Yoon, Yeon Ji Chung, and Myung Soo Kim
Department of Chemistry, Seoul National University, Seoul, Korea

Time-evolution of product ion signals in ultraviolet photodissociation (UV-PD) of singly protonated peptides with an arginine at the N-terminus was investigated by using a tandem time-of-flight mass spectrometer equipped with a cell floated at high voltage. Observation of different time-evolution patterns for different product ion types—an apparently nonstatistical behavior—could be explained within the statistical framework by invoking consecutive formation of some product ions and broad internal energy distributions for precursor ions. $a_n + 1$ and b_n ions were taken as the primary product ions from this type of peptide ions. Spectral characteristics in post-source decay, UV-PD, and collisionally activated dissociation at low and high kinetic energies could be explained via rough statistical calculation of rate constants. Specifically, the striking characteristics in high-energy CAD and UV-PD—dominance of a_n and d_n formed via $a_n + 1$—were not due to the peculiarity of the excitation processes themselves, but due to quenching of the b_n channels caused by the presence of arginine. (J Am Soc Mass Spectrom 2008, 19, 645–655) © 2008 American Society for Mass Spectrometry

Tandem mass spectrometry has been widely used for identification and sequence determination of polypeptides and proteins [1–3]. In spite of extensive studies made so far, fundamental understanding on the dissociation of activated peptide ions observed by tandem mass spectrometry is still lacking. This is in contrast with the case of the dissociation of small polyatomic ions, for which nearly quantitative theoretical description and even prediction are possible [4]. The main reasons for such a lack of fundamental understanding are experimental and computational difficulties to get structural, mechanistic, and kinetic data for large polyatomic systems consisting of more than 100 atoms. In this regard, it is to be mentioned that we recently developed a systematic method to calculate sequence-specific statistical (Rice-Ramsperger-Kassel-Marcus, RRKM) rate constants for dissociations of peptide and protein ions [5–7].

The most popular method to activate a peptide ion and hence to induce its dissociation is the collisionally activated dissociation (CAD) [8–12]. The kinetic energy of a peptide ion is an important factor affecting the CAD spectral pattern. Hence, CAD of a peptide ion is classified into two categories, low (around 100 eV) and high (higher than 1 keV) energy regimes. In the low-energy CAD [11], which is typically done with triple quadrupole ion trap and ion cyclotron resonance mass spectrometers, a peptide ion gains sufficient energy for dissociation usually via multiple collisions, each collision supplying rather small amounts of internal energy through vibrational excitation. Most of the product ions are *b* and *y* types (see Scheme **1**) formed via rearrangement reactions.

Presence of arginine, proline and aspartic acid residues and the charge state of a peptide ion are known to affect the relative intensities of these product ions. The "mobile proton" model [13, 14] has been devised to explain this. In the high-energy CAD [10], which is usually done with sector and time-of-flight (TOF) mass spectrometers, a peptide ion gains more internal energy than the above through electronic excitation. In the case of singly protonated peptides without an arginine residue, most of the product ions are *b* and *y* types, and some *a* type also, just as in low-energy CAD. When an arginine residue is present, a rather dramatic spectral change occurs; *a* and *d* type product ions dominate with an arginine residue at the N-terminus while *x*, *y*, *v*, and *w* types dominate with the same residue at the C-terminus. For the former case, which is related to the main subject of this paper, Biemann and coworkers [15] suggested that *a* and *d* type products were formed via radical site reactions of $a + 1$ type ions generated via simple bond cleavage of the precursor ion.

Photoexcitation is another useful method to activate a peptide ion. Infrared multiphoton dissociation (IRMPD) [16, 17] is widely practiced, especially in trapping type instruments. In IRMPD, internal energy is supplied via sequential multiple vibrational excitations, as in low-energy CAD. Hence, the overall spectral

Address reprint requests to Dr. M. S. Kim, Department of Chemistry, Seoul National University, Seoul 151-742, Korea. E-mail: myungsoo@snu.ac.kr

1044-0305/08/$32.00
doi:10.1016/j.jasms.2008.02.003

Published online February 23, 2008
Received January 2, 2008
Revised February 14, 2008
Accepted February 16, 2008

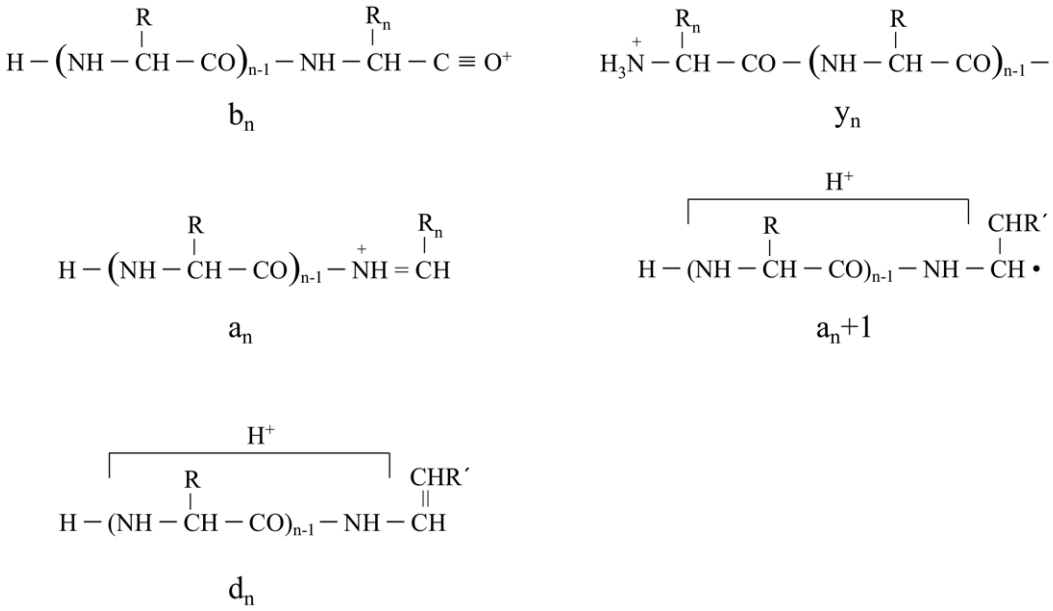

Scheme 1. Structures of the product ions of interest in this work.

feature in IRMPD is rather similar to that in low-energy CAD. Even though photodissociation (PD) by ultraviolet (UV) or vacuum ultraviolet (VUV) light, or UV-PD, has been widely used to study the structure and dissociation dynamics of small polyatomic ions [18, 19], decent tandem mass spectra of peptide ions measured by UV-PD have been reported only recently [20–24]. Ion activation in this technique occurs via electronic excitation, as in high-energy CAD. The fact that the excited electronic state accessed can be controlled by choosing the wavelength is one of the advantages of UV-PD. Tandem mass spectra of singly protonated peptides measured by this technique have been found to be quite similar to those by high-energy CAD [25].

Recently, we reported a new technique [26] to get temporal information on PD of protonated peptides generated by matrix-assisted laser desorption ionization (MALDI). A peptide ion (MH^+) beam was irradiated by 266 nm PD laser beam inside a cell floated at high voltage. Since the final kinetic energies of the same product ions (m_1^+) formed inside (in-cell) and outside (post-cell) the cell differed, the two could be separated by a reflectron analyzer. Also, additional peaks appeared between the two in the TOF spectra. These were due to consecutive formation ($MH^+ \rightarrow m_i^+ \rightarrow m_1^+$) of the product ion via intermediate ions (m_i^+) with the first step occurring inside the cell and the second step outside. A method based on SIMION calculation was developed to estimate the intermediate ion masses. Identification of major consecutive dissociation channels for model peptide ions resulted in fragmentation maps for the photoexcited peptide ions.

Since the main purposes of the previous work were to develop the new technique and to get a spectral overview, peptide ions with an arginine residue—there is some controversy on their dissociation mechanism [21, 23, 27]—were intentionally excluded in the study. With the working principle of the technique well established, we attempted to obtain and analyze the time-resolved PD data for peptide ions with an arginine residue at the N-terminus. Some of the observations, such as different time-evolution patterns for different reactions, were apparently in contradiction with the statistical picture of unimolecular reaction. It has been found, however, that an explanation of the observations within the statistical framework is possible by taking into account the internal energy distributions for peptide ions generated by MALDI and occurrence of consecutive reactions. The results are reported in this paper.

Experimental

Details of the homebuilt tandem TOF instrument and its operation were reported previously [26]. A brief description is as follows. The instrument consists of a MALDI source with delayed extraction, a first-stage TOF analyzer to time-separate the prompt ions generated by MALDI, an ion gate, a PD cell, and a second-stage TOF analyzer equipped with a reflectron. The ion gate is located immediately in front of the first time focus and the PD cell at the first time focus. A deflection system [28] to eliminate fragment ions generated by post-source decay (PSD) is installed between the ion source and the ion gate; 337 nm output from a nitrogen laser (MNL205-C; Lasertechnik Berlin, Berlin, Germany) is used for MALDI; 20 kV DC and 1.8 kV AC pulse are used in the ion source for delayed extraction/acceleration. The potential inside the reflectron has linear and quadratic components. The final electrode of

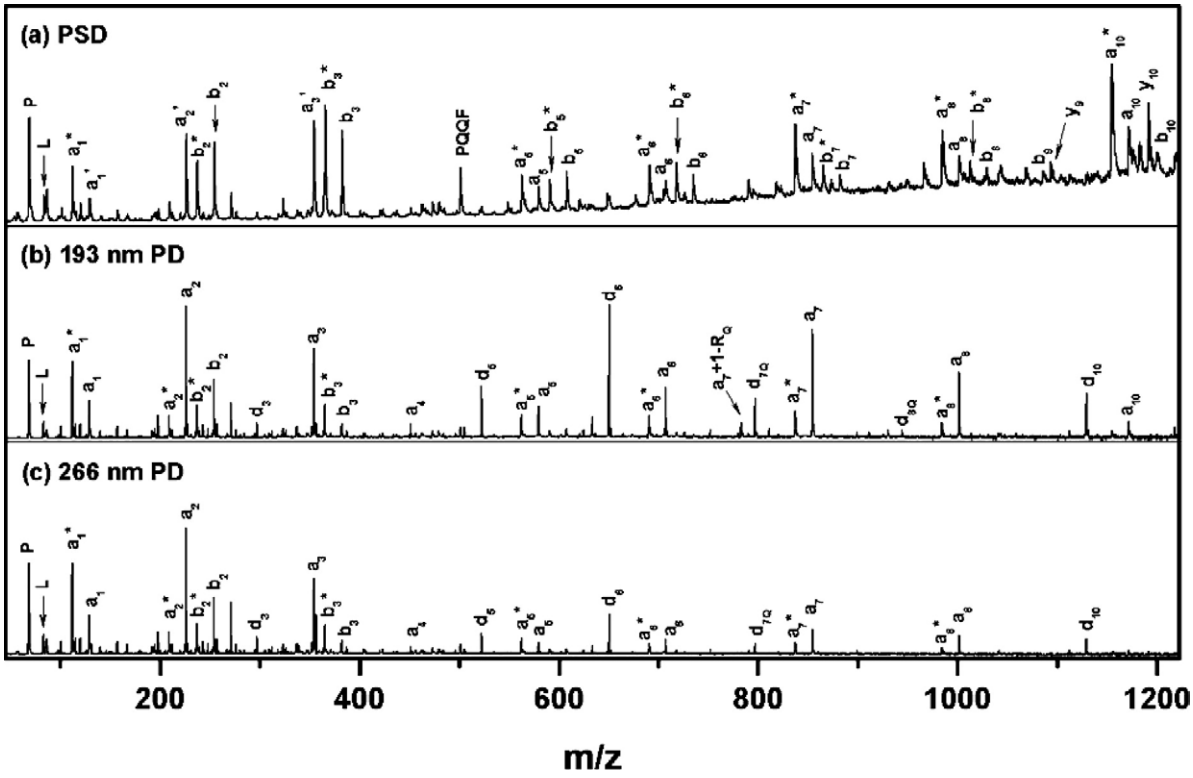

Figure 1. (**a**) PSD, (**b**) 193 nm PD, and (**c**) 266 nm PD spectra of singly protonated substance P. Laser-off spectrum was subtracted from laser-on spectrum to obtain each PD spectrum. a_n* and b_n* indicate a_n-NH_3 and b_n-NH_3, respectively.

the reflectron is kept at 25 kV in normal operation. A pulsed PD laser, either 266 nm output from a Nd:YAG laser (Surelite III-10; Continuum, Santa Clara, CA) or 193 nm output from an ArF excimer laser (PSX-100; MPB Communication Inc., Montreal, Quebec, Canada), is irradiated at the center of the PD cell perpendicularly to the ion beam direction. Two delay generators control timing for MALDI laser irradiation, AC pulsing for delayed extraction, ion gate opening, and PD laser pulsing. The PD laser pulse is synchronized with the A peak (the lowest-mass isotopomer) of the precursor ion selected for PD. PD laser intensity is set such that intensity-dependent spectral change is insignificant. The PSD spectrum under the same experimental condition is recorded without the PD laser pulse. The output from the MCP detector is digitized by an A/D card and treated to minimize electrical noise [29]. Finally, the laser-off spectrum (PSD) is subtracted from the laser-on spectrum to obtain the laser-induced change or the PD spectrum.

RLLAPITAY and RVYIPF with better than 90% purity were purchased from Peptron (Daejon, Korea). Substance P (RPKPQQFFGLM-NH_2) with better than 98% purity, the matrix (α-cyano-4-hydroxycinammic acid), and other chemicals were purchased from Sigma (St. Louis, MO). A matrix solution prepared daily using acetonitrile and 0.1% trifluoroacetic acid was mixed with a peptide solution. The final peptide concentration prepared for PD experiment was 10 pmol/μL; 1 μL of the solution was loaded on the sample plate. The method to prepare a deuterated MALDI sample is the same as above except that D_2O (better than 99.96% isotopic purity) was used as the solvent. A sample plate was placed inside the sample introduction system, which was flushed with D_2O, evacuated by a rotary pump, and then filled with dry nitrogen. Peptide/matrix mixture was loaded on the plate through a septum by syringe. The system was evacuated after 1 min and the sample plate was introduced to the ion source.

Results and Discussion

We carried out time-resolved study for several singly protonated peptides with an arginine at the N-terminus. Their characteristics were very similar. Details will be explained here using the singly protonated substance P as an example because rather extensive studies on the fragmentation of this ion in high-energy CAD [15] and in PSD [30] were reported previously. The PSD spectrum of the singly protonated substance P and the PD spectra recorded at 193 and 266 nm are shown in Figure 1. The PSD spectrum looks similar to the one reported by Spengler et al. [30]. Peaks in the PD spectra look sharper than those in PSD. This is because mono isotopomeric selection has been made in PD via synchronization of the laser pulse with the A peak pulse of the ion beam. Even though the intensity patterns in the two PD spectra are somewhat different, product ions

appearing in the two are similar. They are also similar to those appearing in the high-energy CAD spectrum reported by Biemann et al. [15]. Following the previous report by Spengler et al. [30], prominent product ions in the PSD spectrum (Figure 1a) can be assigned to a_n' (n = 1–3), a_n (n = 5–8, 10), a_n-NH_3 (n = 1, 5–8, 10), b_n (n = 2, 3, 5–10), and b_n-NH_3 (n = 2, 3, 5–8); a_n' ions appear at the same m/z as the corresponding a_n ions in the PSD spectrum. From the H/D exchange study, Spengler et al. [30] showed that each a_n' was either a_n-NH_3 + OH or a collection of internal ions. Some y type ions also appear in PSD, y_{10} being the most prominent. In the 193 nm PD spectrum, product ions with m/z assignable to a_n (n = 1–8, 10) appear prominently. Since it is not clear at this point whether the first three in this series are genuine a_n or a_n', they will be denoted a_n. a_n-NH_3 (n = 1, 2, 5–8), b_n (n = 2, 3), and b_n-NH_3 (n = 2, 3) also appear as in PSD. Among the product ions observed in PSD, y type ions are virtually absent in PD. In contrast, d type ions, which were absent in PSD, appear prominently in PD, viz. d_n (n = 3, 5, 6, 10). Other prominent ions are d_{7Q} and a_7 + 1-R_Q. According to Biemann et al. [15], d_{7Q} is formed by the cleavage of the β, γ bond of glutamine from the a_7 + 1 ion and a_7 + 1-R_Q is formed from $(M + H - 72)^+$, viz. loss of the glutamine side-chain from $(M + H)^+$.

When the cell voltage is applied, each product ion peak in a PD-TOF spectrum usually split into more than one components as has been mentioned in the introductory section. The time-of-flight position of each component changes with the applied voltage. After the acquisition of a voltage-on spectrum, it has been our routine to linearly shift its x (time)-scale such that the time-of-flight of the precursor ion peak coincides with that in the voltage-off spectrum. Then, the time-of-flight position of the post-cell component of each product ion, which is due to its formation from the photoexcited precursor ion after the latter ion passes the cell, also coincides with the product ion position in the voltage-off spectrum [26]. This allows ready identification of the post-cell components, or post-cell peaks. The component of a product ion signal in the voltage-on spectrum that displays the largest deviation from the post-cell peak position is usually due to in-cell formation of the ion, while those in-between are due to its consecutive formation. Under the experimental condition used in PD of substance P ion, an in-cell peak is due to product ions formed within 110 ns after photoexcitation, while the corresponding post-cell peak is due to ions formed from the precursor ions during 0.18 to 4.9 μs after photoexcitation. In Figure 2, the peak patterns for a_2, b_2, a_5-NH_3, d_5, and a_7 in the 193 nm PD spectrum recorded with 3 kV cell voltage are compared with those in the voltage-off spectrum. It can be seen that post-cell peaks are stronger than in-cell peaks for a_2, b_2, and a_5-NH_3, while the opposite is the case for a_7. In the case of d_5, post-cell peak is nearly absent. Trends observed for other major peaks also belonged to one of the above three categories; dominant post-cell peaks for low mass a_n (n = 1–3), a_n-NH_3, b_n, and b_n-NH_3, dominant in-cell peaks for high mass a_n (n = 4–8, 10), and mostly in-cell peaks for d_n and d_{7Q}.

Let us first consider a simple situation where all the dissociation channels for the precursor ion M^+ occur competitively and terminate in the first step, viz. consecutive reactions do not occur. Let us denote the rate constant for the production of each first-generation product ion m_j^+ (j = 1 − n), which will be called a primary product ion hereafter, as k_j. Then, the kinetics of formation of each m_j^+ is governed by the total rate constant, which is the sum of k_j, not by the individual rate constant. The individual rate constant k_j only determines the relative intensity of m_j^+. Then, all the primary product ions should show similar time-evolution pattern in the voltage-on spectrum. If consecutive reactions also occur, ions generated from the primary product ions, which will be called the secondary product ions, are not in competition with the primary product ions and can show different time-evolution patterns. Hence, participation of consecutive reactions can be an explanation for the appearance of three different time-evolution patterns in the voltage-on spectrum. However, there can be other explanations also. When one-step reactions of a precursor ion generate two different product ions, one rapidly and the other slowly, one often suspects the participation of nonstatistical processes. Two important assumptions in the statistical theory of mass spectra, RRKM-QET (quasi-equilibrium theory) [31, 32], are rapid internal conversion to the ground electronic state and rapid intramolecular vibrational redistribution (IVR) in the ground electronic state. Whether the dissociation of an electronically excited peptide ion would satisfy the above two conditions has been a subject of controversy [21, 23, 27, 33, 34]. This question must be addressed before attempting to explain the appearance of three apparently different time-evolution patterns.

The electronic transition occurring at 193 nm is probably $\pi_P^* \leftarrow \pi_P$ localized at peptide bonds [21, 35]. The first requirement for RRKM-QET would not be satisfied if the $\pi_P\pi_P^*$ state thus accessed is dissociative. In contrast, the transition at 266 nm is localized at aromatic chromophores, viz. phenylalanine, tyrosine and tryptophan residues. Hence, it is unlikely that the excited-state accessed at 266 nm is also dissociative with respect to peptide bond cleavages. In our previous study [21], and also in Figure 1, we showed that the product ions formed by 193 nm PD were similar to those by 266 nm PD and suggested that the reactions observed occurred in the ground electronic state. As a further test, we recorded the voltage-on PD spectrum at 266 nm. The peak patterns for the same ions as in Figure 2, viz. a_2, b_2, a_5-NH_3, d_5, and a_7 are shown in Figure 3. Clearly, the splitting patterns at 266 and 193 nm are very similar and hence the first requirement for RRKM-QET is probably met.

In one of our previous studies on 266 nm PD of peptide ions, it was observed that some product ions

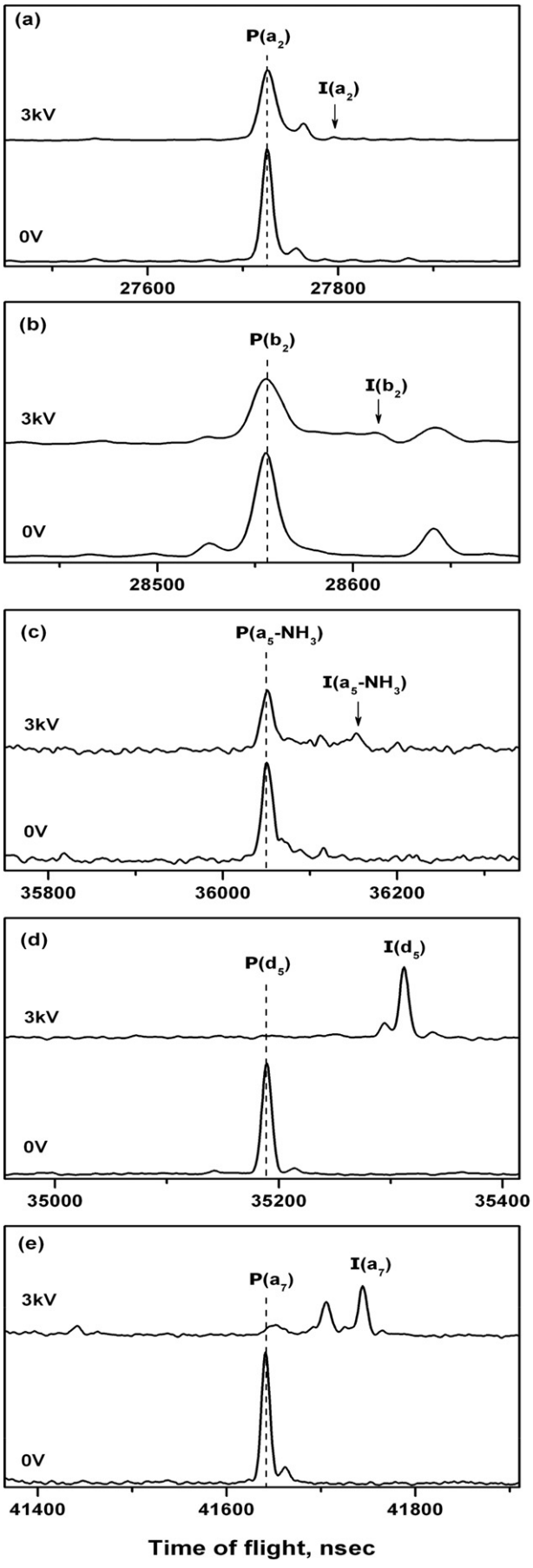

formed by cleavage of peptide bonds immediately adjacent to an aromatic chromophore were particularly prominent [34]. It was suggested that the observation might be explained by postulating two types of dissociation, one occurring before complete IVR and the other after IVR. In this regard, it may be interesting to note that d_n ions show mostly in-cell peaks in the voltage-on spectra. That is, formations of these ions are nearly completed within the cell unlike other product ions, suggesting their possible formation before complete IVR. Evidences against such a possibility can be found from the voltage-on 266 nm PD spectrum of substance P ion. Formation of d_6 is related to the cleavage of the peptide bond connected to the chromophore (F) and is completed rapidly. In contrast, formations of d_3, d_5, and d_{10}, which are also rapidly completed, are related to the cleavage of bonds separated from the chromophore by one or more residues. We also observed post-cell d peaks, even though weak, in 266 nm PD of some peptide ions, such as d_3 and d_{6a} from $[RLLAPITAY + H]^+$. Such observations suggest that rapid or dominant formation of some product ions in UV-PD has nothing to do with incomplete IVR, viz. the second requirement for RRKM-QET is probably met. Based on the above arguments, it should be possible to explain, even though qualitatively, the appearance of three different time-evolution patterns within the statistical framework by taking into account the possibility of consecutive reactions.

Investigations on the dissociation of protonated peptides at low internal energy reported so far suggest that b_n ions are primary product ions [11, 36–43]; a_n ions may be formed via CO loss from b_n [11, 36, 39, 40]. a_n-NH_3 and b_n-NH_3 are other secondary product ions appearing prominently at low internal energy, such as in the PSD spectrum shown in Figure 1a. As has been mentioned already, a_n and d_n are the most prominent product ions in the high-energy dissociation of protonated peptides with an arginine at the N-terminus. According to Biemann et al. [15], d_n is formed from a_n + 1 and a_n from a_n + 1 and b_n. a_n + 1 ions are probably the primary product ions formed via the bond cleavage between C_α and CO, as noted by Reilly et al. [24]. Hence, it seems to be reasonable to postulate that the formations of a_n + 1 and b_n are the primary dissociation channels in direct competition in the present case and that other product ions are formed consecutively. Based on this picture, mostly post-cell formation of a_n-NH_3 and b_n-NH_3 can be readily explained by postulating slow NH_3 loss from a_n and b_n, respectively, or by postulating consecutive reactions via $[MH - NH_3]^+$ [11, 43, 44]. Slow formation of low mass a_n (n = 1–3) can also

Figure 2. The peak patterns for (**a**) a_2, (**b**) b_2, (**c**) a_5-NH_3, (**d**) d_5, and (**e**) a_7 in the 193 nm PD spectrum recorded with 3 kV cell voltage. The patterns recorded without the cell voltage are shown at the bottom of each figure. Vertical dotted lines are drawn at the positions of post-cell (P) peaks. In-cell peaks are marked I.

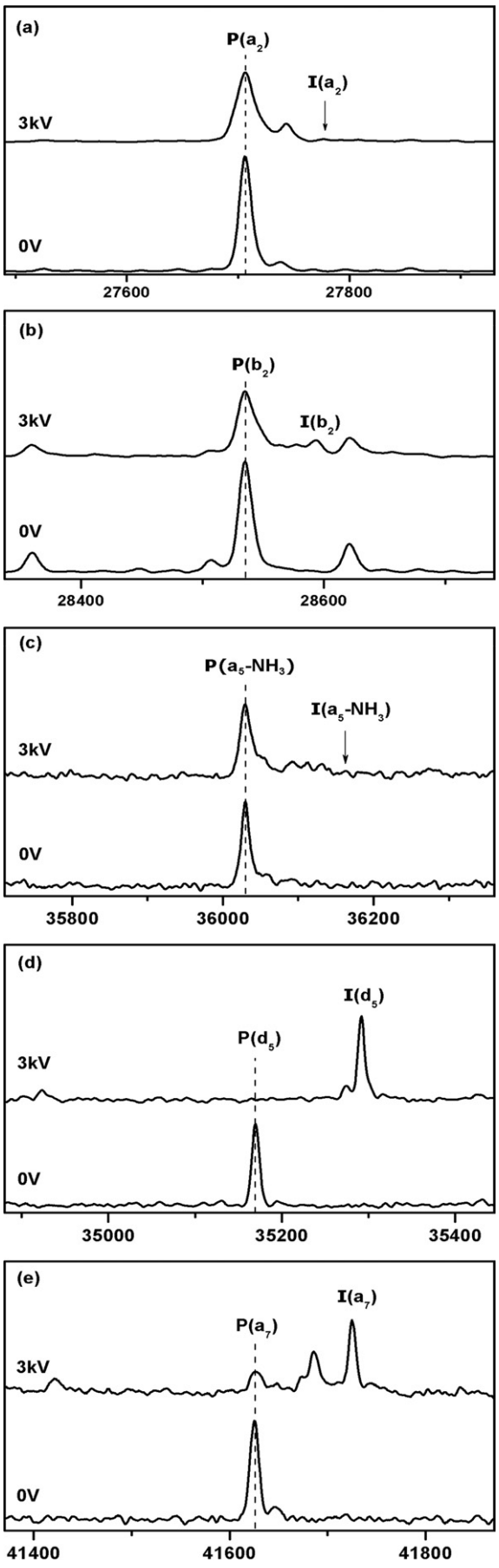

Figure 3. The peak patterns for (**a**) a_2, (**b**) b_2, (**c**) a_5-NH_3, (**d**) d_5, and (**e**) a_7 in the 266 nm PD spectrum recorded with 3 kV cell voltage. The patterns recorded without the cell voltage are shown at the bottom of each figure. Vertical dotted lines are drawn at the positions of post-cell (P) peaks. In-cell peaks are marked I.

be explained by invoking consecutive reactions if these are a_n', not genuine a_n, as found in PSD, even though further confirmation via H/D exchange work is needed.

b_n ions are formed via rearrangement reactions [38–42] with small critical energies (E_0) and small entropies of activation ($\Delta S^{\ddagger}$). In contrast, both E_0 and $\Delta S^{\ddagger}$ are expected to be larger in the formation of $a_n + 1$, which is a simple bond cleavage. As is well known in ion chemistry [4, 18], small E_0 and $\Delta S^{\ddagger}$ processes dominate at low internal energy, but give way to large E_0 and $\Delta S^{\ddagger}$ processes as the internal energy increases. Let us assume that $a_n + 1$, which is a radical cation, dissociates rapidly to a_n and d_n. Then, the striking difference in spectral pattern between PSD and UV-PD shown in Figure 1, that is, dominance of b_n and its products, viz. b_n-NH_3, a_n, and a_n-NH_3 in PSD versus dominance of a_n and d_n in UV-PD, can be easily understood.

The main problem in the above explanation is the fact that two groups of competing primary channels, b_n and $a_n + 1$, seem to occur with noticeably different rate constants, mostly post-cell for the former reactions and mostly in-cell for the latter reactions. This is in apparent contradiction with the fact that the time-evolution patterns for all the competing channels are only governed by the total rate constant and should be the same. We can get out of this dilemma by recognizing that peptide ions generated by MALDI are not monoenergetic but have rather broad internal energy distributions (a sample calculation will be presented later). Accordingly, the internal energy distribution for photoexcited ions will also be broad. For a photoexcited precursor ion with sufficiently high internal energy, formation of $a_n + 1$ will dominate. Such an ion will have a large total rate constant and dissociate rapidly inside the cell. b_n may be formed at low-energy, even though weakly. Small total rate constant in this case would result in slow formation of b_n, mainly outside the cell.

The remaining difficulty concerns the fact that the time-evolution patterns of d_n and high mass a_n ions, which are thought to be formed competitively from $a_n + 1$, are a little bit different. Experiments have consistently shown that the post-cell contribution for high mass a_n, even though very small, is more noticeable than that for d_n. Such a tiny difference may occur because $a_n + 1$ is not monoenergetic. Also to be recalled is that $a_n + 1$ is not the sole precursor for a_n, viz. a_n can also be formed from b_n. To get more information on the nature of a_n ions, both at low and high m/z, we attempted to differentiate these ions through H/D exchange and observe their time-evolution patterns.

At low internal energy, a_n is thought to be formed from b_n via CO loss [39, 40]. The mechanism for the

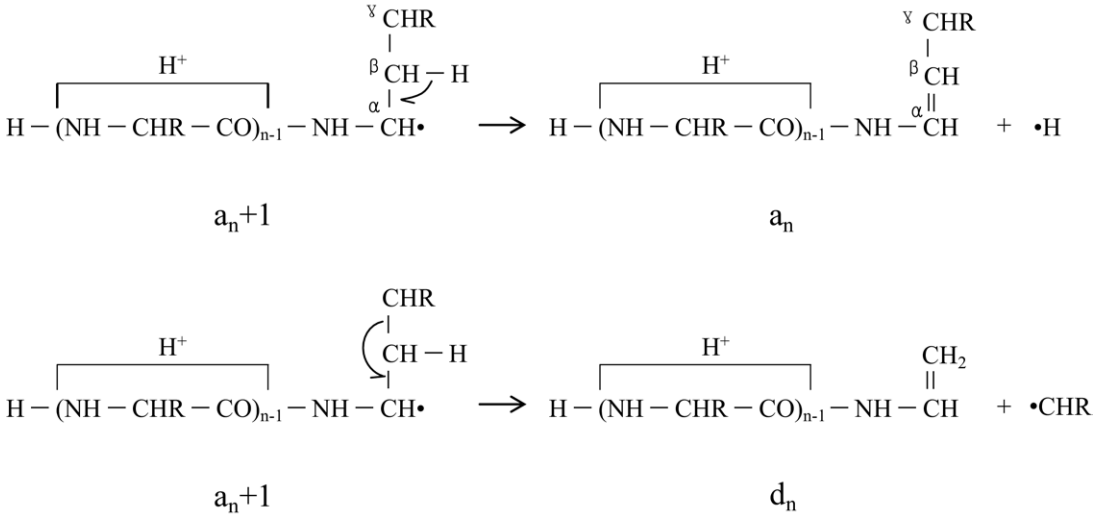

Scheme 2. Another structure of a_n is shown in.

production of b_n from a singly protonated peptide has been actively investigated. The general consensus [38–42] reached is that the additional proton in the precursor ion migrates to the N atoms of amide bonds and the cleavage of these bonds with charge retention in the N-terminal side results in b_n. In this model, the additional proton no longer remains in b_n, and hence neither in a_n. That is, when a deuteron is attached to substance P, this will not be retained in a_n. At high internal energy, a_n + 1 ions are the primary products. Requirement of charge retention in the N-terminal side necessitates presence of the additional proton in the same side, probably at the arginine residue, which is the most basic. Biemann et al. [15] suggested that the radical site initiation at C_α induces homolytic C_β-H or C_β-C_γ cleavage, resulting in a_n or d_n ions as shown in Scheme **2**.

The hydrogen atom at C_β is not acidic and can not be deuterated by simple H/D exchange. Hence, two types of a_n ions can be differentiated by H/D exchange; mass of a_n formed via b_n, or a_n^l, is 1 Da lower than that via a_n + 1, or a_n^h. In the PSD study of deuterated substance P ion reported by Spengler et al. [30], all the high mass a_n ions were found to have the masses of a_n^l. In contrast, those of a_n (n = 1–3) were smaller by 2 Da, suggesting that they were not genuine a_n ions. Reilly et al. [45] also used H/D exchange in their structural study of α-type ions formed by 157 nm PD in ion trap of peptide ions with an arginine at the N-terminus. Two types of a_n ions were observed, designated as a_n + 1-D and a_n + 1-H. The latter ion is a_n^h in our notation. a_n + 1-D, which appears at the same mass as a_n^l, was assumed to be formed via homolytic cleavage of the N–D bond adjacent to C_α. This mechanism was invoked to explain strong a_n ions formed by cleavage at the C-terminal side of a glycine residue which does not have a β hydrogen. It is to be noted that a_n formed at the glycine site of substance P ion, viz. a_9 (m/z 1058.6), is very weak in our PD spectra. As mentioned above, generation of d_n via homolytic C_β-C_γ cleavage is another competitive dissociation channel for a_n + 1. Favorable formation of d_n at glutamic acid, glutamine, isoleucine, leucine, lysine, and valine sites were reported by Biemann et al. [15]. This is in agreement with the observation in the PD spectra obtained in this work (Figure 1).

Substance P has 22 exchangeable hydrogen atoms. Including a deuteron added in ion formation, the mass of substance P ion deuterated by H/D exchange is larger by 23 Da than that of the undeuterated ion. The molecular ion region of the deuterated substance P ion measured by MALDI-TOF in this work is shown in Figure 4. The peak at m/z 1371.0 is the A peak of the deuterated peptide ion. A peak due to incomplete deuteration also appears at 1 Da below. Degree of

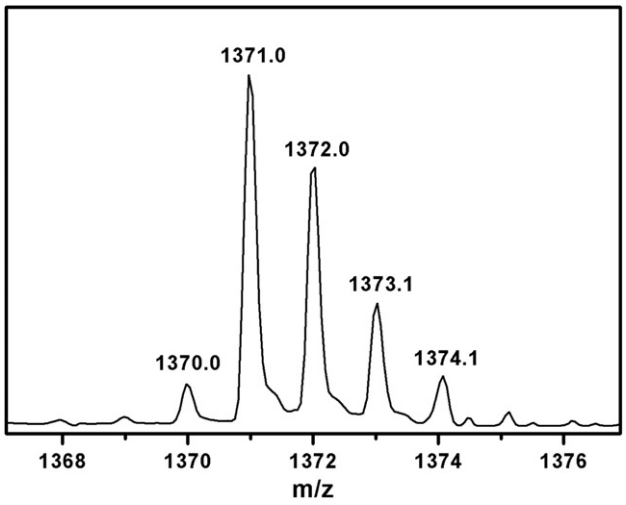

Figure 4. The molecular ion region of the MALDI-TOF spectrum of substance P deuterated by simple H/D exchange. The peak at m/z 1371.0 is the A peak of the deuterated peptide ion.

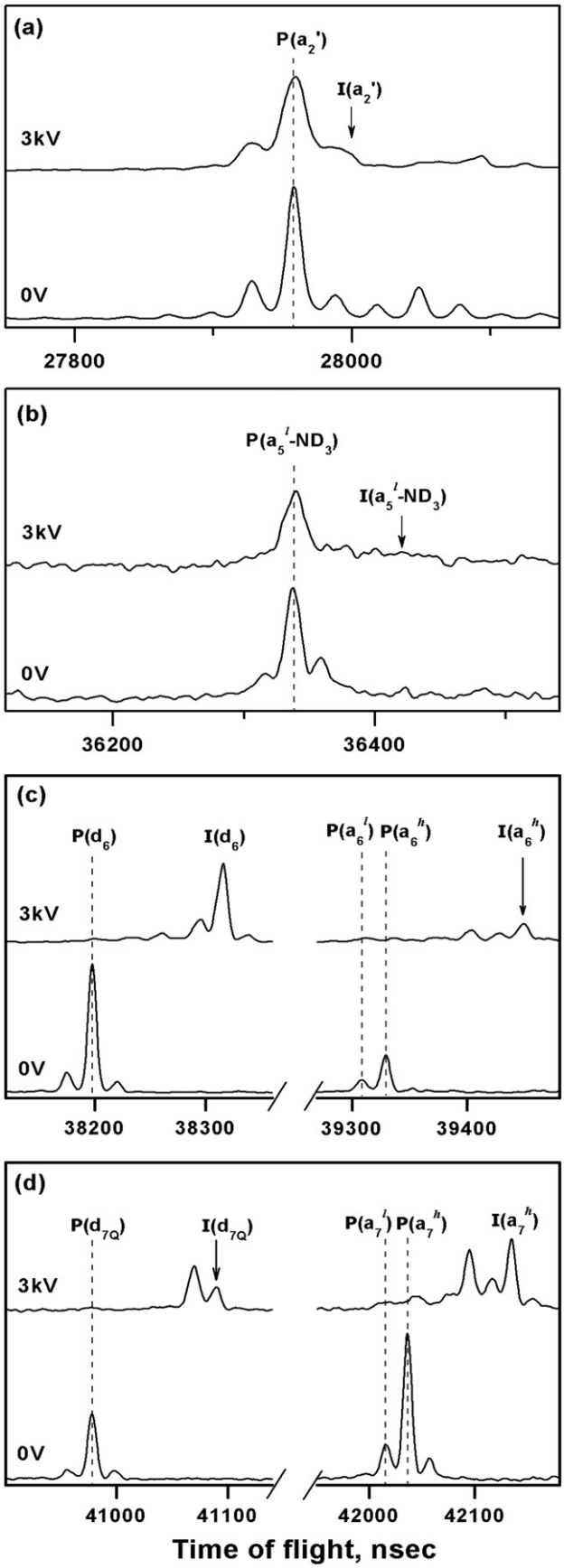

Figure 5. The peak patterns for (**a**) a_2', (**b**) a_5-ND_3, (**c**) (d_6, a_6) pair, and (**d**) (d_{7Q}, a_7) pair in the 193 nm PD spectrum of deuterated substance P recorded with 3 kV cell voltage. The patterns recorded without the cell voltage are shown at the bottom of each figure. Vertical dotted lines are drawn at the positions of post-cell (P) peaks. In-cell peaks are marked I.

deuteration calculated from the isotopic pattern is around 99%.

We recorded 193 nm PD spectrum for the A peak of the deuterated substance P ion. The full spectrum (not shown) is similar to that of the undeuterated ion once mass changes due to deuteration are taken into account. Some differences can be seen when the spectrum is expanded. Figure 5 shows the peak patterns of a_2, a_5-ND_3, (d_6, a_6) pair, and (d_{7Q}, a_7) pair recorded without and with the cell voltage. Mass of the main peak of a_2 (Figure 5a) is smaller than expected for a_n^l by 2 Da, in agreement with Spengler et al. [30]. Then, dominance of the post-cell component for this a_n' may be attributed to its consecutive formation. a_5-NH_3 (Figure 5b) appears at the position expected for a_n^l-ND_3, indicating that some a_n ions are indeed formed from b_n; d_6 (Figure 5c), and d_{7Q} (Figure 5d) appear at the expected positions. Small additional peaks appear at 1 Da below the main peaks in these cases. We do not know whether these additional peaks appear due to the experimental failure in monoisotopomeric selection or due to participation of other reactions. For a_6 (Figure 5c) and a_7 (Figure 5d), peaks corresponding to a_n^l (or a_n + 1-D) and a_n^h are observed. The cell voltage-on patterns show that the post-cell contributions in $a^h{}_6$ and $a^h{}_7$ are very small, almost comparable to those in d_6 and d_{7Q}. The post-cell contributions in $a^l{}_6$ and $a^l{}_7$ (or a_n + 1-D) are also small, but are relatively larger than in a_n^h. The fact that the post-cell contributions in a_n^h and d_n are almost comparable suggests that the pathways leading to these product ions are competing effectively. Considering that the post-cell contribution for the peak at 1 Da smaller mass is not large, it is unlikely that a_n^l formed from b_n is the sole contributor to this peak. Sole contribution from a_n + 1-D is unlikely either because its post-cell contribution is not as important as for a_n^h. These peaks may be combinations of a_n^l and a_n + 1-D. The important thing is that separating these peaks from a_n^h results in rather similar time-evolution patterns for a_n^h and d_n. We also performed 193 nm PD for a few other deuterated peptide ions. Peak patterns of d_{4a} and a_4 from $[RVYIPF + D]^+$ are shown in Figure 6. Here again, the post-cell contribution in a_n^h is very small while that at 1 Da lower is much larger.

We have suggested that dissociation of an electronically excited peptide ion with an arginine at the N-terminus, either in UV-PD or in high-energy CAD, occurs statistically in the ground state. Two sets of channels, simple homolytic cleavages to a_n + 1 (high E_0 and high $\Delta S^{\ddagger}$) and rearrangement reactions to b_n (low E_0 and low $\Delta S^{\ddagger}$), were assumed to be in competition. A

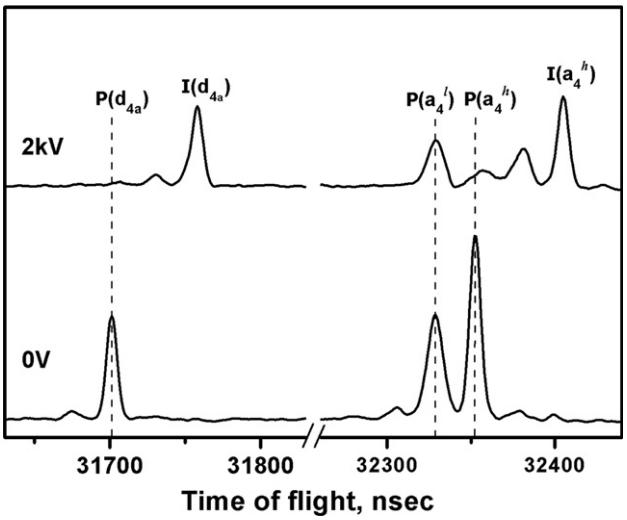

Figure 6. The peak patterns for d_{4a} and a_4 in the 193 nm PD spectrum of deuterated $[RVYIPF + D]^+$ recorded with 2 kV cell voltage. The patterns recorded without the cell voltage are shown at the bottom of the figure. Vertical dotted lines are drawn at the positions of post-cell (P) peaks. In-cell peaks are marked I.

broad internal energy distribution for a photoexcited peptide ion originating from the thermal energy acquired at the time of ion formation (MALDI) was invoked to explain the different time-evolution patterns for these two channels. For a rigorous test of this model, accurate data on internal energy distribution and rate constants are needed, which are not available at the moment. In the theoretical estimation of the rate-energy (k(E)) data, particularly troublesome is the b_n channel, which is thought to occur along a reaction pathway consisting of several isomerization/tautomerization steps [38, 46]. It is uncertain how the rate constant in each step would influence the overall rate constant. Since the main purpose of the present effort was just to demonstrate the feasibility of the statistical picture in explaining the experimental observations, a drastically simple approach was taken. That is, the statistical dissociation rate constants to $a_n + 1$ and b_n for substance P ions were calculated by RRKM-QET as if each of them occurred via a hypothetical one-step reaction. The software reported previously [5–7] was used in the calculation. The software also calculates the internal energy distribution for a precursor ion at a specified temperature. Since the software in its present form can handle regular peptides and peptide ions only, not amide derivatives such as substance P, a minor adjustment would be needed. This has not been made in this work because the outcomes are expected to be nearly the same regardless of the adjustment. As the reaction coordinate, a mode at 1150 cm^{-1}, which is a default in the software, was chosen. Use of other modes did not noticeably affect the rate-energy (k(E)) curve.

It is usual to treat peptide ions generated by MALDI as if they were in thermal equilibrium [47, 48]. To calculate the internal energy distribution of a peptide ion with this model, its effective temperature is needed. It is a parameter that can not be easily measured. Also, it may change significantly depending on the MALDI condition used. It can be anywhere between 500 and 1000 K, or even higher [47, 49]. The parameters needed to calculate the rate-energy curve for each channel are E_0 and $\Delta S^{\ddagger}$. None of these parameters are accurately known for $a_n + 1$ and b_n channels. From quantum chemical studies, Paizs and Suhai [38, 39] suggested E_0 of 0.65 to 1.1 eV for *b-y* dissociation channels for peptide ions without an arginine residue. No theoretical study has been reported for *b-y* channels for peptide ions with this residue. It is thought that a statistical description of this case would require an E_0 value larger than the arginine-free case. In an $a_n + 1$ channel, a C–C bond is broken. Its E_0 may be smaller than the typical C–C bond energy of 345 kJ mol^{-1} (3.6 eV) due to stabilization of the radical sites in the ionic and neutral products. In dissociation of small molecules, $\Delta S^{\ddagger}$ for a reaction occurring via a tight transition-state (rearrangement) is near 0 eu (1 eu = 4.184 J K^{-1} mol^{-1}) while that via a loose transition-state (simple bond cleavage) is near 15 eu [31, 33]. $\Delta S^{\ddagger}$ for $a_n + 1$ channels may be even larger considering the complexity of peptide ions. Keeping in mind the main purpose of the present effort, we took freedom in choosing values for the above parameters.

To calculate the k(E) curve for a b_n channel in substance P ion, we used $E_0 = 1.4$ eV and $\Delta S^{\ddagger} = 0.0$ eu. Then, k(E) thus obtained for a single b_n channel was multiplied by 10 to mimic participation of many such channels. Similar calculation was done for $a_n + 1$ channels using $E_0 = 2.0$ eV and $\Delta S^{\ddagger} = 20$ eu. The results are shown in Figure 7. Change in the dominant channel, from b_n at low-energy to $a_n + 1$ at high-energy, can be seen in the figure. The rate constant estimated from the flight time of a photoexcited ion inside the cell is marked in the figure. This is approximately the minimum rate constant needed for in-cell dissociation. The rate constant range for the appearance of PSD is also marked in the figure; 700 K was taken as the effective temperature of substance P ion generated by MALDI. Its internal energy distributions before and after the absorption of one 193 nm photon are also shown in Figure 7. It can be seen from the figure that b_n channels dominate in PSD, which is driven by the internal energy acquired in MALDI. With the addition of one 193 nm photon, rapid in-cell dissociation can occur mostly via $a_n + 1$ channels, even though slower post-cell dissociation via b_n channels is also possible for photoexcited ions with internal energy falling in the lower part of the distribution. The overall situation is in agreement with the statistical interpretation presented in this paper. We do not claim that k(E) and energy distribution curves shown in Figure 7, the magnitude of each parameter used in particular, are correct descriptions of the situation. By using other sets of parameters, we could obtain results that were compatible with observations. The point here is that it is possible to explain the different dissociation patterns for a peptide ion with an arginine

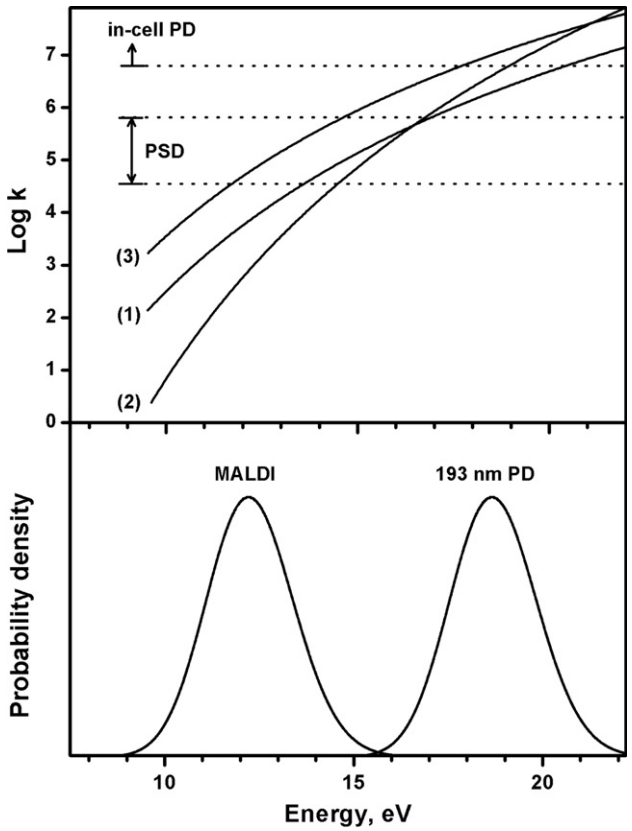

Figure 7. k(E) curves for dissociation of substance P ions calculated with (1) E_0 = 1.4 eV, $\Delta S^{\ddagger}$ = 0.0 eu, (2) E_0 = 2.0 eV, $\Delta S^{\ddagger}$ = 20 eu, and (3) E_0 = 1.28 eV, $\Delta S^{\ddagger}$ = 0.0 eu. (1) and (2) are model calculations for b_n and a_n + 1 channels, respectively; (3) is a fictitious model for b_n channels in the absence of arginine. The internal energy distributions for the same ion before (marked as MALDI) and after (marked as 193 nm PD) absorption of one 193 nm photon are shown at the bottom; 700 K was taken as the effective temperature of the ion generated by MALDI.

at the N-terminus, PSD versus UV-PD or low versus high-energy CAD, within the statistical framework.

We have mentioned earlier that characteristic patterns in UV-PD, and also in high-energy CAD , were observed for peptide ions with an arginine residue. For peptide ions without this residue [11, 39], b_n and y_n ions dominated just as in PSD and low-energy CAD. We were curious to know whether such an insensitivity of the spectral pattern could also be explained within the statistical framework. Use of an E_0 value in the theoretically predicted range 0.65 to 1.1 eV [39] was found to be inadequate because k(E) thus obtained predicted complete disappearance of the precursor ion by PSD. To avoid this, we calculated k(E) using E_0 = 1.28 eV and $\Delta S^{\ddagger}$ = 0.0 eu. The result is also shown in Figure 7. In this case, b_n channels dominate almost over the entire energy range covered, in agreement with experimental observations. This suggests that the striking characteristics in high-energy CAD and UV-PD—dominance of a_n and d_n—of peptide ions with an arginine at the N-terminus are not due to the peculiarity of the excitation processes themselves, but due to quenching of the dominant low-energy channels caused by the presence of arginine. It is also to be noted that a slight difference in E_0, 1.40 versus 1.28 eV in the present calculations, can lead to the dramatic difference in spectral pattern between peptide ions with and without an arginine, even though the internal energies of activated peptide ions are as large as 20 eV.

Conclusions

Substantially different time-evolution patterns for different product ion types were observed in UV-PD experiments for singly protonated peptides with an arginine residue at the N-terminus using a voltage-floated cell, as if nonstatistical processes had participated. Additional experiments indicated, however, that dissociations occurred statistically in the ground electronic states. The apparent conflict could be reconciled by invoking that some product ions were formed via consecutive reactions and that peptide ions generated by MALDI had a rather broad internal energy distribution. It was suggested that rearrangement reactions to b_n and homolytic cleavages to a_n + 1 were the first step dissociation channels which were in competition in the energy range covered. Feasibility of this model was demonstrated through rough internal energy and RRKM calculations. The results were compatible with the observations that b_n channels were dominant in PSD and low-energy CAD while a_n + 1 channels became important in UV-PD and high-energy CAD. In the case of peptide ions without an arginine residue, a sample calculation predicted dominance of b_n channels over the entire energy range covered, again in agreement with observations. Specifically, the striking characteristics in high-energy CAD and UV-PD—dominance of a_n and d_n—of peptide ions with an arginine at the N-terminus were not due to the peculiarity of the excitation processes themselves, but due to quenching of the dominant low-energy channels caused by the presence of arginine.

Present statistical calculations were made under the dramatically simplistic assumption of one-step reaction for each channel. They also suffer from the lack of knowledge on the internal energy distribution for peptide ions and dynamical parameters governing their dissociation. We hope that the reliability of the statistical calculation will improve with further investigations, both experimental and theoretical. Then, one may be able to check the participation of an alternative nonstatistical mechanism by comparing with statistically expected results.

Acknowledgments

The authors gratefully acknowledge financial support for this work by the Korea Research Foundation, Republic of Korea, and by the Biosignal Analysis Technology Innovation program (M10645010002-06N4501-00,210) of the Ministry of Science and

Technology, Republic of Korea. SHY and YJC thank the Ministry of Education, Republic of Korea, for Brain Korea 21 Fellowship.

References

1. Mann, M.; Hendrickson, R. C.; Pandey, A. Analysis of Proteins and Proteomes by Mass Spectrometry. *Annu. Rev. Biochem.* **2001**, *70*, 437–473.
2. Kinter, M.; Sherman, N. E. *Protein Sequencing and Identification Using Tandem Mass Spectrometry*; John Wiley: New York, 2000; pp. 64–116, pp. 238–268.
3. Hernandez, P.; Müller, M.; Appel, R. D. Automated Protein Identification by Tandem Mass Spectrometry: Issues and Strategies. *Mass Spectrom. Rev.* **2006**, *25*, 235–254.
4. Bowers, M. T., Ed. In *Gas Phase Ion Chemistry, Vol. III, Ions and Light*, Eds.; Academic Press: Orlando, FL, 1984.
5. Moon, J. H.; Oh, J. Y.; Kim, M. S. A Systematic and Efficient Method to Estimate the Vibrational Frequencies of Linear Peptide and Protein Ions with Any Amino Acid Sequence for the Calculation of Rice-Ramsperger-Kassel-Marcus Rate Constant. *J. Am. Soc. Mass Spectrom.* **2006**, *17*, 1749–1757.
6. Sun, M.; Moon, J. H.; Kim, M. S. Improved Whitten-Rabinovitch Approximation for the Rice-Ramsperger-Kassel-Marcus Calculation of Unimolecular Reaction Rate Constant for Proteins. *J. Phys. Chem. B* **2007**, *111*, 2747–2751.
7. Moon, J. H.; Sun, M.; Kim, M. S. Efficient and Reliable Calculation of Rice-Ramsperger-Kassel-Marcus Unimolecular Reaction Rate Constants for Biopolymers: Modification of Beyer-Swinehart Algorithm for Degenerate Vibrations. *J. Am. Soc. Mass Spectrom.* **2007**, *18*, 1063–1069.
8. McLafferty, F. W.; Ed. *Tandem Mass Spectrometry*, Wiley-Interscience: New York, 1983; pp 125–174.
9. Cooks, R. G. 1978; Collision-Induced Dissociation of Polyatomic Ions. Cooks, R. G., Ed.; In Collision Spectroscopy; pp 375–450.Plenum: New York,
10. Martin, S. A.; Biemann, K. 1990, Sequencing of Peptides by Tandem Mass Spectrometry and High-Energy Collision-Induced Dissociation. McCloskey, J. A., Ed.; In Methods in Enzymology, Vol. CXCIII, Mass Spectrometry; pp 455–479.Academic Press: New York,
11. Medzihradszky, K. F. 2005, Peptide Sequence Analysis. Burlingame, A. L., Ed.; In Methods in Enzymology, Vol. CDII, Biological Mass Spectrometry; pp 209–244.Academic Press: San Diego,
12. Laskin, J.; Futrell, J. H.; Collisional Activation of Peptide Ions in FT-ICR Mass Spectrometry. *Mass Spectrom. Rev.* **2003**, *22*, 158–181.
13. Wysocki, V. H.; Tsaprailis, G.; Smith, L. L. Breci, L. A. Mobile and Localized Protons: A Framework for Understanding Peptide Dissociation. *J. Mass Spectrom.* **2000**, *35*, 1399–1406.
14. Summerfield, S. G.; Whiting, A.; Gaskell, S. J. Intra-Ionic Interactions in Electrosprayed Peptide Ions. *Int. J. Mass Spectrom. Ion Processes* **1997**, *162*, 149–161.
15. Johnson, R. S.; Martin, S. A.; Biemann, K. Collision-Induced Fragmentation of $(M + H)^+$ Ions of Peptides. Side Chain Specific Sequence Ions. *Int. J. Mass Spectrom. Ion Processes* **1988**, *86*, 137–154.
16. Little, D. P.; Sper, J. P.; Senko, M. W.; O'Connor, P. B.; McLafferty, F. W. Infrared Multiphoton Dissociation of Large Multiply Charged Ions for Biomolecule Sequencing. *Anal. Chem.* **1994**, *66*, 2809–2815.
17. Laskin, J.; Futrell, J. H. Activation of Large Ions in FT-ICR Mass Spectrometry. *Mass Spectrom. Rev.* **2005**, *24*, 135–167.
18. Bowers, M. T., Ed.; *Gas Phase Ion Chemistry, Vol. II*, Eds.; Academic Press: New York, 1979; pp 181–220.
19. Dunbar, R. C. Photodissociation of Trapped Ions. *Int. J. Mass Spectrom.* **2000**, *200*, 571–589.
20. Moon, J. H.; Yoon, S. H.; Kim, M. S. Photodissociation of Singly Protonated Peptides at 193 nm Investigated with Tandem Time-of-Flight Mass Spectrometry. *Rapid Commun. Mass Spectrom.* **2005**, *19*, 3248–3252.
21. Choi, K. M.; Yoon, S. H.; Sun, M.; Oh, J. Y.; Moon, J. H.; Kim, M. S. Characteristics of Photodissociation at 193 nm of Singly Protonated Peptides Generated by Matrix-Assisted Laser Desorption Ionization (MALDI). *J. Am. Soc. Mass Spectrom.* **2006**, *17*, 1643–1653.
22. Barbacci, D. C.; Russell, D. H. Sequence and Side-Chain Specific Photofragment (193 nm) Ions from Protonated Substance P by Matrix-Assisted Laser Desorption Ionization Time-of-Flight Mass Spectrometry. *J. Am. Soc. Mass Spectrom.* **1999**, *10*, 1038–1040.
23. Thompson, M. S.; Cui, W.; Reilly, J. P.Fragmentation of Singly Charged Peptide Ions by Photodissociation at $\lambda = 157$ nm.Angew. Chem. Int. Ed. 2004 43 4791–4794.
24. Cui, W.; Thompson, M. S.; Reilly, J. P. Pathways of Peptide Ion Fragmentation Induced by Vacuum Ultraviolet Light. *J. Am. Soc. Mass Spectrom.* **2005**, *16*, 1384–1398.
25. Moon, J. H.; Shin, Y. S.; Cha, H. J.; Kim, M. S. Photodissociation at 193 nm of Some Singly Protonated Peptides and Proteins with *m/z* 2000-9000 Using a Tandem Time-of-Flight Mass Spectrometer Equipped with a Second Source for Delayed Extraction/Post-Acceleration of Product Ions. *Rapid Commun. Mass Spectrom.* **2007**, *21*, 359–368.
26. Yoon, S. H.; Kim, M. S. Development of a Time-Resolved Method for Photodissociation Mechanistic Study of Protonated Peptides: Use of a Voltage-Floated Cell in a Tandem Time-of-Flight Mass Spectrometer. *J. Am. Soc. Mass Spectrom.* **2007**, *18*, 1729–1739.
27. Morgan, J. W.; Russell, D. H. Comparative Studies of 193-nm Photodissociation and TOF-TOFMS Analysis of Bradykinin Analogues: The Effects of Charge Site and Fragmentation Timescales. *J. Am. Soc. Mass Spectrom.* **2006**, *17*, 721–729.
28. Yoon, S. H.; Moon, J. H.; Choi, K. M.; Kim. M. S. A Deflection System to Reduce the Interference from Post-Source Decay Product Ions in Photodissociation Tandem Time-of-Flight Mass Spectrometry. *Rapid Commun. Mass Spectrom.* **2006**, *20*, 2201–2208.
29. Moon, J. H.; Yoon, S. H.; Kim. M. S. Enhancement of Matrix-Assisted Laser Desorption/Ionization Photodissociation Tandem Time-of-Flight Mass Spectra: Spectral Reduction and Cleanup of Isotopomeric Contamination. *Rapid Commun. Mass Spectrom.* **2005**, *19*, 2481–2487.
30. Spengler, B.; Lützenkirchen, F.; Kafumann, R. On-Target Deuteration for Peptide Sequencing by Laser Mass Spectrometry. *Org. Mass Spectrom.* **1993**, *28*, 1482–1490.
31. Baer, T.; Hase, W. L. *Unimolecular Reaction Dynamics: Theory and Experiments*, Eds.; Oxford University Press: New York, 1996; pp 171–415.
32. Holbrook, K. A.; Pilling, M. J.; Robertson, S. H. Unimolecular Reactions; Wiley: Chichester, 1996; pp 39–78
33. Hu, Y.; Hadas, B.; Davidovitz, M.; Balta, B.; Lifshitz, C. Does IVR Take Place Prior to Peptide Ion Dissociation? *J. Phys. Chem. A* **2003**, *107*, 6507–6514.
34. Oh, J. Y.; Moon, J. H.; Kim, M. S. Sequence- and Site-Specific Photodissociation at 266 nm of Protonated Synthetic Polypeptides Containing a Tryptophanyl Residue. *Rapid Commun. Mass Spectrom.* **2004**, *18*, 2706–2712.
35. Robin, M. B. *Higher Excited States of Polyatomic Molecules, Vol. II*, Eds.; Academic Press: New York, 1974; pp 122–155.
36. Papayannopoulos, I. A. The Interpretation of Collision-Induced Dissociation Tandem Mass Spectra of Peptides. *Mass Spectrom. Rev.* **1995**, *47*, 49–73.
37. Kaufmann, R.; Spengler, K. B. Sequencing of Peptides in a Time-of-Flight Mass Spectrometer: Evaluation of Post-Source Decay Following Matrix-Assisted Laser Desorption Ionization. *Int. J. Mass Spectrom. Ion Processes* **1994**, *131*, 355–385.
38. Paizs, B.; Suhai, S. Combined Quantum Chemical and RRKM Modeling of the Main Fragmentation Pathways of Protonated GGG. II. Formation b_2, y_1, and y_2 Ions. *Rapid Commun. Mass Spectrom.* **2002**, *16*, 375–389.
39. Paizs, B.; Suhai, S. Fragmentation Pathways of Protonated Peptides. *Mass Spectrom. Rev.* **2005**, *24*, 508–548.
40. El Aribi, H.; Rodriquez, C. F.; Almeida, D. R. P.; Ling, Y.; Mak, W. W.-N.; Hopkinson, A. C.; Siu, K. W. M. Elucidation of Fragmentation Mechanisms of Protonated Peptide Ions and Their Products: A Case Study on Glycylglycylglycine Using Density Functional Theory and Threshold Collision-Induced Dissociation. *J. Am. Chem. Soc.* **2003**, *125*, 9229–9236.
41. Polce, M. J.; Ren, D.; Wesdemiotis, C. Dissociation of the Peptide Bond in Protonated Peptides. *J. Mass Spectrom.* **2000**, *35*, 1391–1398.
42. Schlosser, A.; Lehmann, W. D. Five-Membered Ring Formation in Unimolecular Reaction of Peptides: A Key Structural Element Controlling Low-Energy Collision-Induced Dissociation of Peptides. *J. Mass Chem.* **2000**, *35*, 1382–1390.
43. Laskin, J.; Bailey, T. H.; Futrell, J. H. Mechanisms of Peptide Fragmentation from Time- and Energy-Resolved Surface-Induced Dissociation Studies: Dissociation of Angiotensin Analogs. *Int. J. Mass Spectrom.* **2006**, *249/250*, 462–472.
44. Subra, G.; Aubagnac, J. L.; Martinez, J.; Enjalbal, C. Tandem Mass Spectrometry of Amidated Peptides. *J. Mass Spectrom.* **2006**, *41*, 1470–1483.
45. Zhang, L.; Cui, W.; Thompson, M. S.; Reilly, J. P. Structures of α-Type Ions Formed in the 157 nm Photodissociation of Singly-Charged Peptide Ions. *J. Am. Soc. Mass Spectrom.* **2006**, *17*, 1315–1321.
46. Rodriquez, C. F.; Cunje, A.; Shoeib, T.; Chu, I. K.; Hopkinson, A. C.; Siu, K. W. M. Proton Migration and Tautomerism in Protonated Triglycine. *J. Am. Chem. Soc.* **2001**, *123*, 3006–3012.
47. Zenobi, R.; Knochenmuss, R. Ion Formation in MALDI Mass Spectrometry. *Mass Spectrom. Rev.* **1998**, *17*, 337–366.
48. Dreisewerd, K. The Desorption Process in MALDI. *Chem. Rev.* **2003**, *103*, 395–425.
49. Koubenakis, A.; Frankevich, V.; Zhang, J.; Zenobi, R. Time-Resolved Surface Temperature Measurement of MALDI Matrices under Pulsed UV Laser Irradiation. *J. Phys. Chem. A* **2004**, *108*, 2405–2410.